




Research Paper

Optimized Design and Performance Enhancement of Concentrated Winding BLDC Motors for Aircraft Actuators

Reza Ghanizadeh* , Taher Mohammadi , and Farhad Razavi 

Department of Electrical Engineering, Urmia Branch, Islamic Azad University, Urmia, Iran.

Abstract— Permanent magnet brushless DC (BLDC) motors are increasingly preferred in industrial applications, particularly for low- and medium-power scenarios, due to their commutator-free operation, higher efficiency, reduced maintenance, compact size, and versatile speed control. This work presents the development of an enhanced BLDC motor prototype with concentrated windings, specifically tailored for aircraft actuator applications. The primary objective is to maximize electromagnetic torque and torque per kilogram through a novel dimensional optimization approach. A systematic design procedure, incorporating sensitivity analysis and finite element method (FEM) modeling, was established to identify and optimize key parameters affecting overall performance. Our results demonstrate significant improvements in power density, torque-to-weight ratio, and efficiency compared to conventional designs, offering a robust solution for the demanding requirements of aerospace applications.

Keywords—Brushless DC motor, motor design, optimization, sensitivity analysis, finite element analysis.

1. INTRODUCTION

Brushless DC (BLDC) motors have emerged as a dominant choice in various industrial applications due to their numerous advantages over traditional motors. Despite their efficiency and compactness, ongoing challenges persist, particularly in optimizing winding configurations and minimizing cogging torque [1]. These challenges are exacerbated in applications like aircraft actuators, where high torque density, reliability, and compactness are critical. The superior efficiency, compactness, and competitive pricing of BLDC motors make them indispensable in sectors such as military, aerospace, automotive, and consumer electronics [1]. Their small size correlates with high torque output per kilogram and high power density, which are critical attributes for these demanding applications [2]. The relentless pursuit of higher efficiency in electric motors by manufacturers and researchers is driven by the need to produce more shaft power with less input power. Enhancing motor efficiency can significantly reduce energy costs, extend the operational time of battery-powered devices, and minimize heat generation, thereby boosting reliability and reducing maintenance costs [3]. Improved efficiency also results in lower internal power losses and higher power density since power loss directly affects the motor's temperature rise, a key performance limiter. Concentrated windings, however, offer a simpler structure, resulting in more cost-effective manufacturing processes [4]. These windings also allow for more compact motor

designs due to shorter end-windings and axial build [5]. In [6], the optimal design of permanent magnet brushless DC (BLDC) motors for electromobility applications was explored, employing the Taguchi method alongside finite element analysis. In [7], a newly designed systematic multiphysics multilevel optimization algorithm has been introduced for a BLDC motor, accounting for manufacturing tolerances and driving cycles. In [8], the effect of varying air flow rates on the temperature rise and efficiency of a 500 W BLDC motor during operation was analyzed, providing insights into optimizing cooling strategies for enhanced motor performance. In recent years, the design and analysis of brushless DC (BLDC) motors have gained significant attention due to their potential for enhanced performance in various applications. One significant issue with concentrated winding machines is cogging torque, but studies have shown, it is possible to minimize this without skewing the slots, which in turn increases the machine's power density [9]. In [10], the Multi-Objective Generalized Normal Distribution Optimization method was developed and applied to optimize the design of BLDC motors, outperforming other optimization techniques in achieving optimal efficiency and minimal motor mass. Radial permanent magnet motors, including BLDC motors, are increasingly utilized across various industries such as aerospace, medical, automotive, and industrial automation [11, 12]. The control of these motors often employs field-oriented control (FOC), a technique that simplifies the control design by transforming a three-phase time and speed-dependent system into a two-axis (d-q) coordinate system [13]. This transformation reduces the complexity of control equations and enhances the precision of motor control. In applications requiring rapid acceleration and deceleration, a high torque-to-inertia ratio is desirable [14]. The design and selection of motor phases, poles, stator slots, and winding configurations are crucial and must align with the specific application requirements. Factors influencing the choice of pole number include inertia requirements, magnet material, cogging effects, and rotation speed [11, 14]. While BLDC motors are gaining prominence due to their efficiency and compactness, there are ongoing challenges and areas for improvement, particularly

Received: 21 Jul. 2024

Revised: 27 Nov. 2024

Accepted: 01 Dec. 2024

*Corresponding author:

E-mail: reza.ghanizadeh@iau.ac.ir (R. Ghanizadeh)

DOI: 10.22098/joape.2025.15488.2190

This work is licensed under a [Creative Commons Attribution-NonCommercial 4.0 International License](https://creativecommons.org/licenses/by-nc/4.0/).

Copyright © 2025 University of Mohaghegh Ardabili.

in optimizing winding configurations and minimizing cogging torque. Continued research and development in these areas are essential to fully realize the potential of BLDC motors in various high-performance applications. This paper aims to explore these aspects further, focusing on design improvements and performance optimizations to enhance the applicability and efficiency of BLDC motors in modern industry.

This study focuses on the development of an enhanced Permanent Magnet Brushless DC (BLDC) motor prototype designed for aircraft actuator applications. By implementing a novel dimensional optimization approach, the work aims to maximize electromagnetic torque and torque per kilogram. A systematic design procedure using sensitivity analysis and FEM modeling was applied, leading to significant improvements in power density, torque-to-weight ratio, and efficiency over conventional designs, making it a promising solution for aerospace requirements.

2. DESIGN OF THE PROPOSED BLDC

2.1. Finite element analysis setup

The proposed BLDC motor design process began with the selection of an interior-rotor configuration, which is known for its high torque-to-inertia ratio. Three motor configurations with varying pole numbers were modeled using ANSYS/Maxwell software. Finite Element Analysis (FEA) was employed to simulate electromagnetic behavior under different design conditions. Sensitivity analysis was conducted to determine the impact of key parameters on performance, with the results informing the final optimization step. The optimization process aimed to maximize torque and efficiency and minimize motor weight. The selection of phases, poles, stator slots, and winding configuration must align with the specific needs of the application. The determination of the number of poles is influenced by several factors, including inertia requirements, magnet material, cogging effects, and rotational speed. Doubling the number of poles results in halving the necessary thickness of both the stator and rotor back iron.

Fig. 1 illustrates the finite element model (FEM) of the proposed BLDC motor, developed and analyzed using ANSYS/Maxwell software. The finite element method is a powerful computational technique used to simulate and predict the behavior of complex physical systems, particularly in the context of electromagnetic and electromechanical devices such as BLDC motors. The motor includes 24 slots and 20 poles. The initial dimensions and parameters from the motor design for the desired nominal speed of 300 RPM and a nominal torque of 20 Nm are provided in Table 1.

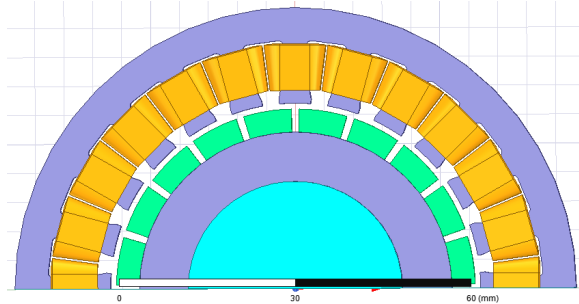


Fig. 1. 2-D finite element model of the BLDC.

2.2. Design equations

The torque in electric motors is generated by the changing magnetic energy within the air gap. This magnetic energy stems from the magnetic field created by current in the coils or permanent magnets, which produce magnetic flux loops in the motor's magnetic materials. Using a magnetic circuit model under

assumptions of linearity in materials and collinearity of flux and field densities, torque generation can be described effectively [15]. Magnetic flux in each branch of the motor circuit can be calculated with air-gap flux density as:

$$B_g(\alpha, \gamma) = \mu_0 \left(\frac{F(\alpha, \gamma)}{l_g(\alpha, \gamma)} \right) \quad (1)$$

Where, F denotes the stator and rotor magnetomotive forces, l_g represents air-gap length, μ_0 is free space permeability, δ is the rotor shift, and α denotes the outer coordinate on the circumference of a circle with the mean radius. Torque distribution is given by:

$$T(\delta) = \int_{R_{in}}^{R_{out}} \frac{\partial W'}{\partial \delta} r dr \quad (2)$$

where, R_{out} and R_{in} indicate the outer and inner radius of the proposed motor, respectively. W' denotes coenergy and is written as Eq. (3) using the outer (R_o) and inner radius (R_i) of the stator.

$$W'(\delta) = (R_{out} - R_{in}) \int_0^{2\pi R} B_g(\alpha, \delta) F(\alpha, \delta) d\alpha \quad (3)$$

The air-gap length, comprising the stator and rotor side air gaps, is given as follows:

$$l_g(\alpha, \delta) = l_{gs}(\alpha, \delta) + l_{gr}(\alpha, \delta) \quad (4)$$

The stator-side effective air-gap length is specified as [16].

$$l_{gs}(\alpha) = \frac{l_g}{1 - s(1 - \cos(2\pi\alpha/\beta))} \quad (5)$$

$$\beta = \frac{kl_g}{s} \quad (6)$$

$$s = \frac{(1 - \tau)^2}{2(1 + \tau^2)} \quad (7)$$

$$k = \frac{4}{\pi} \left[\rho \tan^{-1} \rho - \frac{1}{2} \ln(1 + \rho^2) \right] \quad (8)$$

$$\tau = \rho + \sqrt{1 + \rho^2} \quad (9)$$

$$\rho = \frac{w_s}{2l_g} \quad (10)$$

where l_g represents the smallest air-gap length between the stator and rotor, and w_s denotes the stator slot width. The rotor-side air-gap length l_{gr} depends on the magnet fraction q_m ; it spans $d_r/2$ across the non-magnetic section and is estimated $d_r/(2\mu_r)$ over the magnet width w_m , where the recoil permeability is μ_r . Clearly, the air-gap length distribution is directly influenced by the geometric design parameters. Magnetomotive force is expressed as the sum of the forces from the stator and rotor.

$$F(\alpha, \delta) = F_s(\alpha, \delta) + F_r(\alpha, \delta) \quad (11)$$

Each stator winding generates a magnetomotive force F_s , which is uniformly allocated along the stator shoe. The number of turns per pole is given by n_s , and the conductor carries a current I . Similarly, the magnet's magnetomotive force, F_r , is distributed evenly across its surface, where H_c indicates the magnet's coercivity, and l_r specifies its thickness.

2.3. Selecting pole numbers

To achieve an accurate estimation of the magnetic field distribution within the motor, which is crucial for calculating the induced back EMF and the resulting electromagnetic torque, we have analyzed and presented back-EMF curves for three distinct pole configurations by Matlab/Simulink software in Fig. 2. These curves serve as a critical tool for understanding how variations in the number of poles affect the motor's overall performance. The back-EMF is a key parameter in BLDC motors as it directly influences the generated torque and the efficiency of the motor. By examining these curves, we gain valuable insights into the relationship between the number of poles and the shape of the back-EMF waveform. Specifically, the figures reveal that a motor with a 22-pole configuration produces a back-EMF waveform that closely resembles a trapezoidal shape.

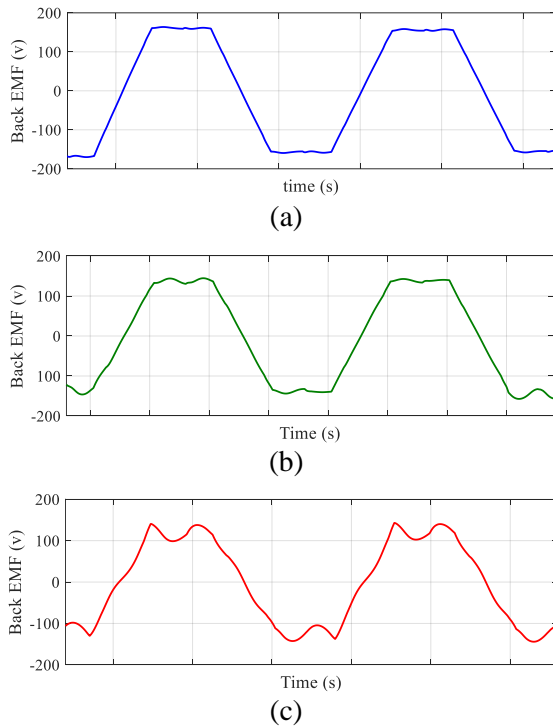


Fig. 2. Back EMF comparison in three different pole numbers, (a) 22, (b) 20, (c) 16.

The cogging torque comparison for three different pole numbers is shown in Fig. 3. According to the curves, the 20-pole configuration shows a reduction in cogging torque amplitude compared to the 16-pole configuration, while the 22-pole configuration exhibits the lowest amplitude. This is due to the increased number of poles, which helps to distribute the magnetic forces more evenly around the stator, thereby reducing the peaks in cogging torque.

The higher cogging torque can lead to greater vibrations and noise, which may negatively affect the smoothness of operation. Fig. 4 presents a comparison of the torque ripple across three distinct motor configurations, each with a different number of poles. Torque ripple, which refers to the variations in torque during motor operation, plays a critical role in determining the smoothness and efficiency of motor performance. Excessive torque ripple can lead to vibrations, noise, and reduced overall efficiency, making minimizing it a key objective in motor design. The figure clearly illustrates how different pole configurations impact the magnitude of torque ripple. As shown in the charts, the motor configuration with 22 poles demonstrates the lowest level of torque ripple among the three structures, which is essential for applications requiring

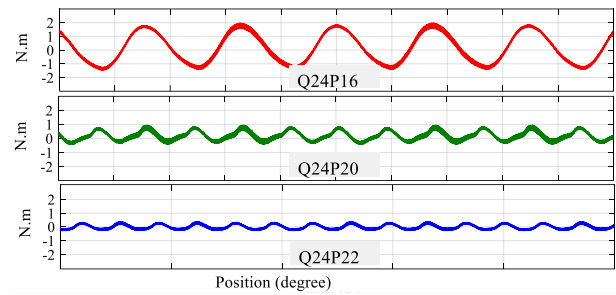


Fig. 3. Cogging torque comparison for three different pole numbers.

high precision and smooth operation.

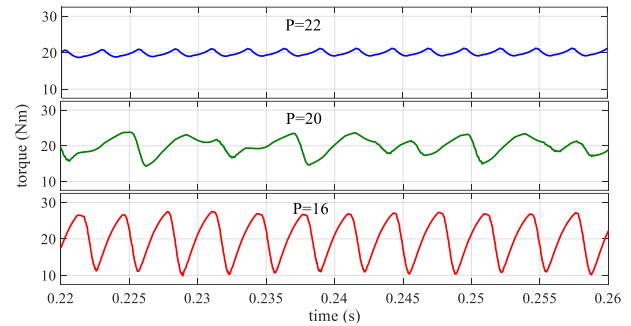


Fig. 4. Torque ripple comparison.

A higher pole count in a BLDC motor results in a more intricate distribution of the magnetic field within the stator. As the pole count grows, the MMF waveform becomes increasingly distorted from the ideal sinusoidal form, leading to the generation of higher-order harmonics. Consequently, the presence of these harmonics becomes more pronounced with an increasing number of poles. The specific harmonic orders in the stator MMF are depicted in Fig. 5.

3. OPTIMIZATION OF THE BLDC

3.1. Performance sensitivity

The design and performance of a Brushless DC (BLDC) motor are inherently linked to its geometric configuration and the characteristics of the magnetic circuit. Traditionally, the initial design of such motors has been guided by fundamental electromagnetic principles and accumulated industry experience, while finite-element analysis (FEA) has been employed for refining and validating the final motor configuration. However, a systematic optimization of the motor's design can yield substantial improvements in efficiency, weight reduction, torque enhancement, and frequency response optimization. These performance metrics are determined by a set of electromagnetic equations, which are functions of the motor's dimensions, material properties, and electrical parameters.

A) Importance and types of sensitivity analysis

Conducting a sensitivity analysis is a crucial step in the design optimization process, as it helps identify the influence of various design parameters on the motor's performance. Sensitivity analysis can be classified into local and global approaches, with local sensitivity focusing on small perturbations around a nominal point, and global sensitivity considering the impact of parameters over a wide range of values. In this study, a local sensitivity analysis is employed using Ansys/Maxwell software to assess how variations in design parameters affect the torque, torque density, and efficiency of the BLDC motor.

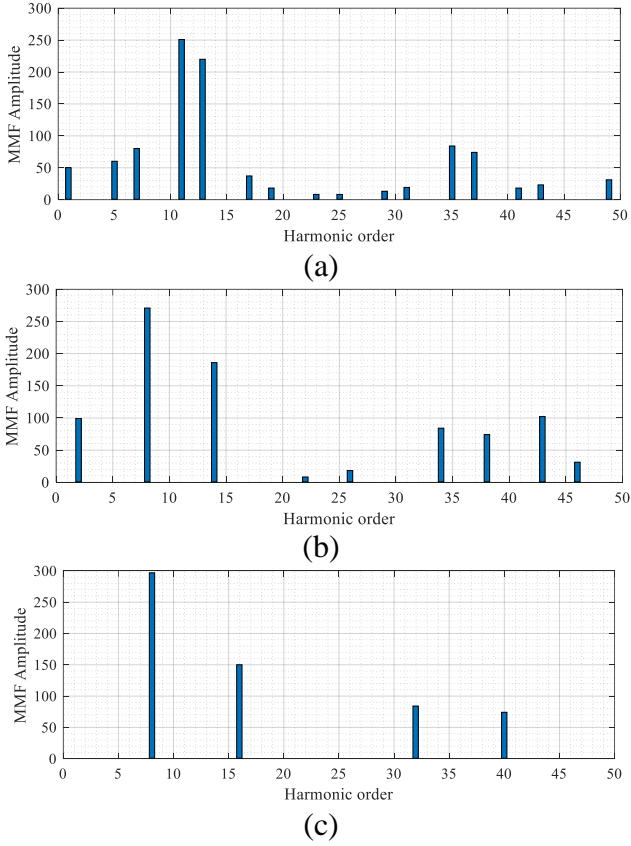


Fig. 5. Special harmonics at different pole numbers.

B) Parameter descriptions and selection ranges

The design parameters considered in this study include the stator inner radius, airgap length, rotor back iron thickness, stator slot coverage, and other critical dimensions that directly impact the electromagnetic performance of the motor. Table 1 outlines the initial values and constraints for these parameters. The selection of parameter ranges was informed by practical design considerations and the need to balance competing objectives such as minimizing losses while maximizing torque and efficiency. For instance, the airgap length was varied between 0.5 mm and 2 mm, as this range reflects the trade-off between mechanical tolerances and electromagnetic coupling efficiency.

C) Computational approach to sensitivity analysis

The sensitivity analysis was conducted using a detailed finite-element model in Ansys/Maxwell, which accurately represents the BLDC motor's electromagnetic behavior under varying design conditions. The software was configured to simulate the motor's performance under steady-state conditions, with particular attention given to the magnetic circuit's response to changes in design parameters. The analysis involved perturbing each design parameter within its specified range while holding other parameters constant at their maximum value, allowing for the isolation of each parameter's impact on performance metrics such as torque and efficiency.

D) Assumptions and limitations

This study assumes linear material properties and neglects temperature effects, which can influence the magnetic properties of the motor's materials. While these assumptions simplify the analysis, they may introduce limitations, particularly under extreme operating conditions. Future studies could incorporate non-linear material models and thermal effects to provide a more comprehensive sensitivity analysis.

Table 1. Initial parameters and constraints.

| Parameter | Symbol | Initial value | constraints |
|--------------------------|----------|---------------------|-------------|
| Number of slots | N_s | 24 | - |
| Number of magnets | N_p | 22 | - |
| Length of motor | l | 100 mm | - |
| Airgap length | g | 1 mm | 0.5 – 2 mm |
| Stator inner radius | r_{is} | 40 mm | 20 – 60 mm |
| Stator outer radius | r_{os} | 67 mm | - |
| Rotor back iron | b_r | 8 mm | 2 – 15 mm |
| Stator slot coverage | f_{ss} | 0.3 | 0.1 – 0.5 |
| Stator tooth coverage | f_{st} | 0.45 | 0.3 – 0.65 |
| Magnet coverage | M_f | 0.5 mm | 0.3 – 0.7 |
| Number of winding layer | N_{lw} | 2 | 1 – 7 |
| Number of turns of layer | N_{lt} | 24 | 10 – 40 |
| Current density | J | 10A/mm ² | - |

E) Assumptions and limitations

This study assumes linear material properties and neglects temperature effects, which can influence the magnetic properties of the motor's materials. While these assumptions simplify the analysis, they may introduce limitations, particularly under extreme operating conditions. Future studies could incorporate non-linear material models and thermal effects to provide a more comprehensive sensitivity analysis.

Figs. 6 and 7 illustrate the sensitivity of motor efficiency and torque to various design parameters. A detailed examination of these curves reveals the critical role of certain parameters, such as the stator inner radius and airgap length, in determining motor efficiency. For example, an increase in the stator inner radius generally enhances the motor's efficiency by reducing flux leakage, while variations in airgap length significantly impact both torque production and efficiency. Conversely, the thickness of the rotor back iron and the stator tooth coverage show a lesser impact on motor torque, indicating that these parameters may be optimized primarily for weight reduction rather than performance enhancement. Non-linear sensitivity behaviours were also observed in certain parameters, suggesting complex interactions between design variables that warrant further exploration. For instance, the sensitivity of efficiency to the number of winding layers is non-linear, with diminishing returns observed as the number of layers increases beyond a certain point. Based on the sensitivity analysis, several design variables with minimal impact on key performance metrics were identified and subsequently fixed or excluded from the optimization process. This refinement reduces the complexity of the optimization task, allowing for a more focused and efficient search for an optimal design. Variables with linear or monotonic sensitivities, such as the stator slot coverage, were also considered for potential optimization but were kept constant during the initial phase to simplify the design process.

3.2. Optimization procedure

The optimization method represents both coenergy and torque through discrete models.

$$\begin{aligned}
 W'(\delta) = & (R_{out} - R_{in}) \int_0^{2\pi R} B_g(\alpha, \delta) F(\alpha, \delta) d\alpha \cong \\
 & \frac{\mu_0(R_o^2 - R_i^2)\Delta\theta}{2} \sum_1^N \frac{F^2(m, \varepsilon)}{l_g(m, \varepsilon)}
 \end{aligned} \quad (12)$$

$$\begin{aligned}
 T(\delta) \cong & \left[W'(\varepsilon + 1) - \frac{W'(\varepsilon)}{\Delta\theta} \right] \Big|_{i=\text{constant}}, \quad m \text{ and } \varepsilon = 1, 2, 3, \dots \quad (13)
 \end{aligned}$$

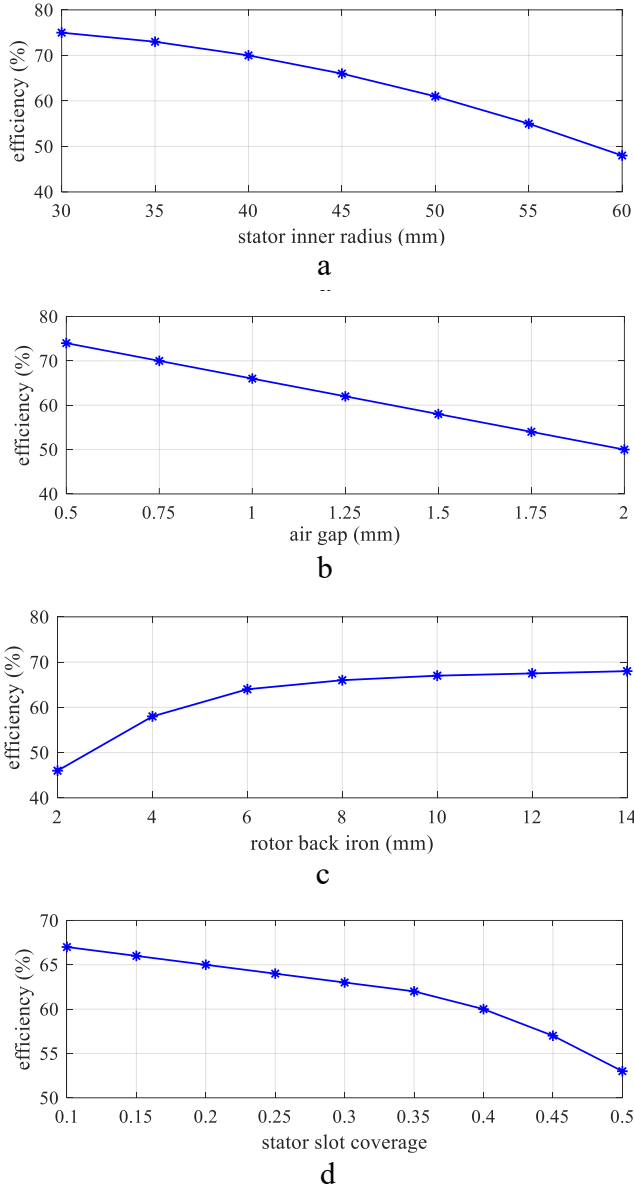


Fig. 6. Sensitivity of efficiency to design parameters, (a) stator inner radius, (b) airgap, (c) rotor back iron, (d) stator slot coverage.

An electrical cycle is partitioned into uniformly distributed points, with each point separated by a constant mechanical angle $\Delta\theta$, defined as $\delta = \varepsilon\Delta\theta$ and $\Delta\alpha = R\Delta\theta$. The compromise programming approach within the multifunctional optimization system tool (MOST) [17] was utilized to identify the optimal design variable values that maximize the following performance indices:

$$T_{nom} : \text{motor nominal torque} \quad (14)$$

$$\tau = 1/W, \text{ } W \text{ is the motor weight} \quad (15)$$

$$\eta = \frac{T_{av}\omega_{rm}}{T_{av}\omega_{rm} + P_{\Omega} + P_c + P_a} \times 100\% \quad (16)$$

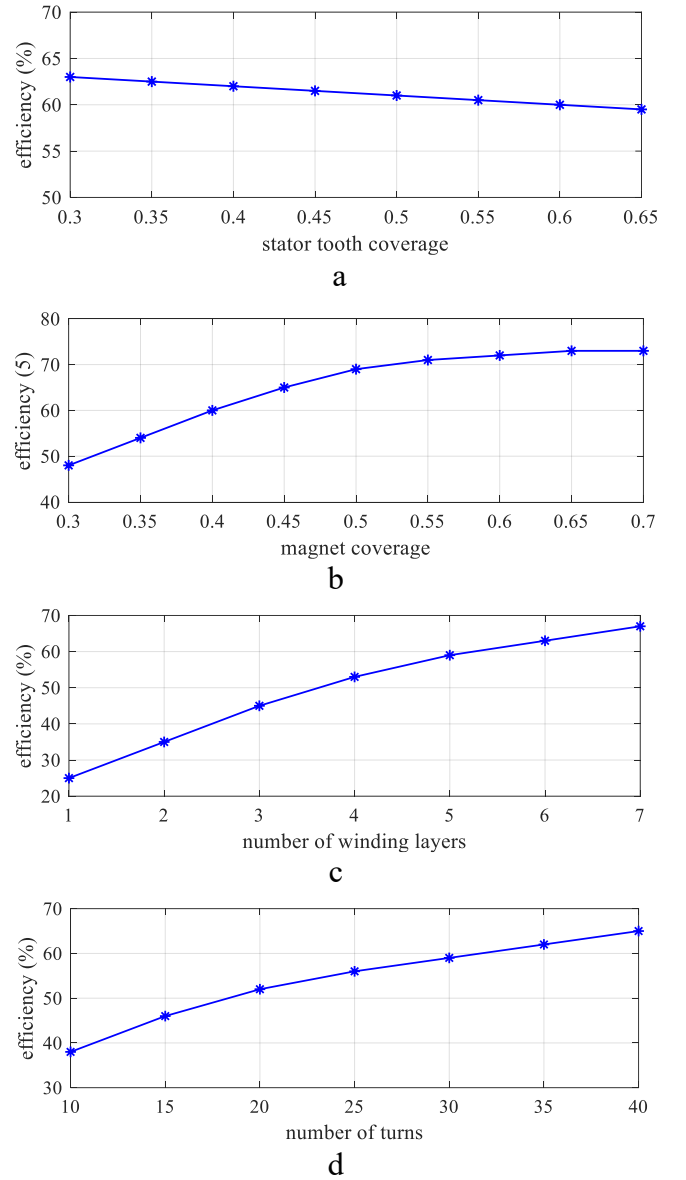


Fig. 7. Sensitivity of efficiency to design parameters, (a) stator tooth coverage, (b) magnet coverage, (c) winding layers, (d) wiring turns.

$$\omega_{nom} : \text{motor nominal speed} \quad (17)$$

where, P_{Ω} , P_c , and P_a are copper loss, iron loss, and additional loss including friction and windage losses, converter transistor losses, and diode losses, respectively. η is the efficiency of the motor and T_{av} denotes the average torque, which is calculated as a function of the design variables in an implicit manner. Assuming linear variations of the field and energy between R_{in} and R_{out} , this integral can be approximated as Eq. (18). This calculation is based on 60 evenly distributed points of rotor displacement over one electrical period, as derived from Eq. (2) [16].

$$T_e(\delta) = (R_{out} + R_{in}) \left. \frac{\partial w'(\delta)}{\partial \delta} \right|_{i=\text{constant}} \quad (18)$$

The optimizer MOST is capable of handling real, integer, and discrete design variables at the same time. In this design scenario, performance indices, design functions, and specified constraints

Table 2. Dimensions at various optimization weights.

| $T_{nom} : \tau : \eta : \omega_{nom}$ | 1:1:1:1 | 1:4:1:1 | 0:2:1:0 |
|--|---------|---------|---------|
| Airgap length (mm) | 0.9 | 1.1 | 1 |
| Stator inner radius (mm) | 43 | 48 | 46 |
| Stator outer radius (mm) | 65 | 67 | 65 |
| Rotor back iron (mm) | 7.2 | 8.7 | 8.1 |
| Stator slot coverage | 0.3 | 0.3 | 0.32 |
| Stator tooth coverage | 0.44 | 0.45 | 0.45 |
| Magnet thickness (mm) | 12.3 | 13.1 | 10.9 |
| Magnet coverage | 0.5 | 0.5 | 0.51 |
| Number of winding layer | 2 | 2 | 2 |
| Number of turns of layer | 28 | 24 | 29 |
| Maximum torque (N.m) | 25 | 21 | 21 |
| Weight of motor (N) | 19.6 | 16.2 | 17.3 |
| Nominal efficiency % | 87 | 86 | 86 |
| Maximum speed (rpm) | 475 | 530 | 414 |
| Torque density | 1.54 | 1.33 | 1.28 |

are represented in terms of design variables. For instance, the number of windings layers and turns per layer are integers and other variables are real numbers. In the proposed gradient-based optimization algorithm in MOST, initially, an estimation of design variables is performed. Subsequently, the gradients for objective and constraint functions are calculated. Next, the maximum descent direction is determined, and the design parameters are updated. Finally, a convergence test is conducted until the final solution is achieved. Various weightings were applied to the three performance indices Eqs. (6) to (9) to reflect their relative importance during the optimization process. Table 2 showcases the top three outcomes in terms of motor performance. From Table 2, it is evident that the weighting ratio of 1:1:1:1 yields the highest maximum torque among the three ratios considered. On the other hand, the motor weight is minimized in the 1:4:1:1 scenario, as this ratio heavily emphasizes weight reduction. The optimal motor speed is also achieved with the 1:4:1:1 ratio. However, the highest torque density is found with the 1:1:1:1 weighting.

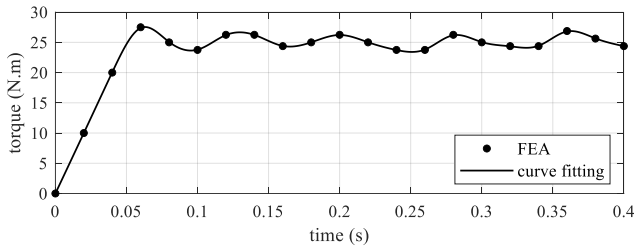


Fig. 8. Torque obtained by finite element analysis for ratio 1:1:1:1.

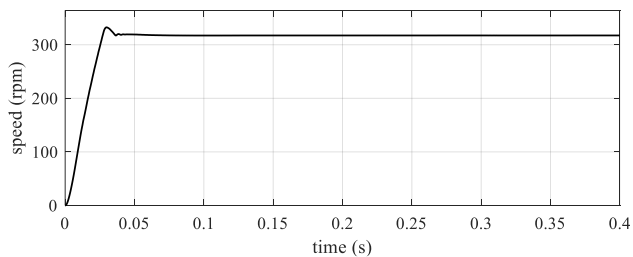


Fig. 9. Speed profile of the motor at start.

4. EVALUATION OF RESULTS

Accurately predicting motor performance using the conventional magnetic circuit model is often challenging. This is due to

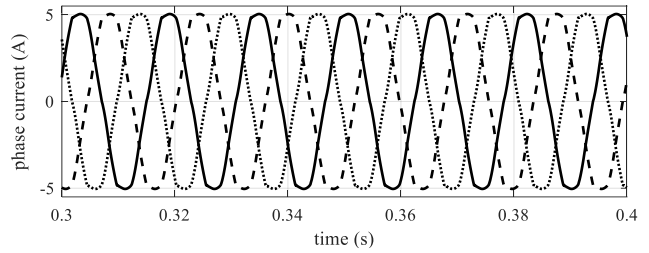
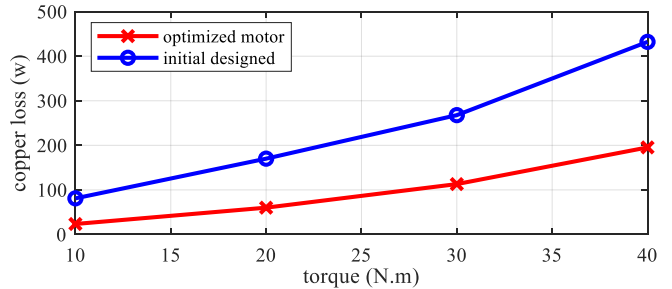
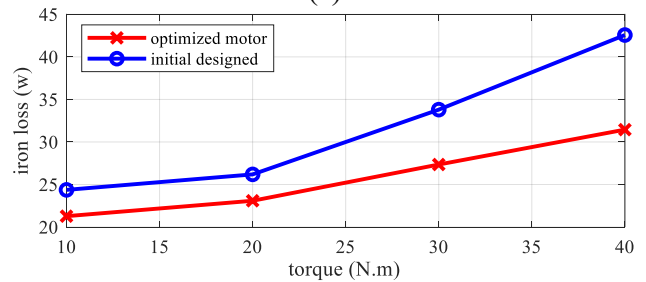


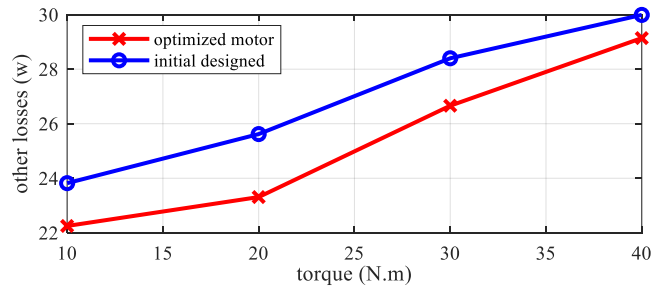
Fig. 10. Phase current of the motor in a time interval.



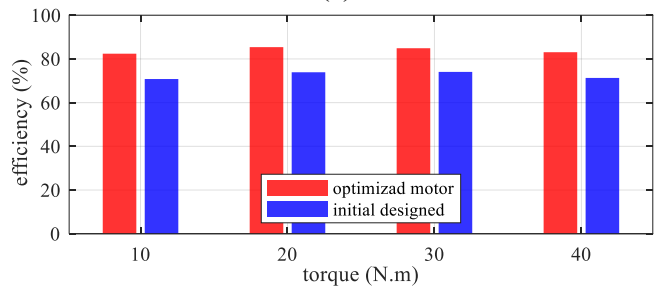
(a)



(b)



(c)



(d)

Fig. 11. Losses comparison, (a) copper loss, (b) iron loss, (c) other losses, (d) efficiency.

several factors: first, the motor in question has a fractional number of slots per pole per phase, which necessitates additional

assumptions and simplifications during magnetic circuit analysis. Second, the nonlinear properties of magnetic materials result in saturation under overload conditions, such as when an electric vehicle is accelerating or climbing a slope. Therefore, finite-element analyses (FEA) on the preliminary design prototype are essential to provide detailed insights into magnetic flux and torque distribution, steady-state temperature distribution, and modal dynamics. These analyses enable designers to evaluate whether additional performance specifications are met or if further iterative design and modifications are required.

Unlike magnetic circuit analysis, the finite-element tool Ansys/Maxwell calculates numerically the magnetic field for the 3-D motor configuration. The finite-element mesh is automatically generated to compute the distributions of magnetic flux, flux density, and torque. The model's boundary is surrounded by air of sufficient thickness, where the magnetic permeability is much smaller than that of magnetic materials. Initially, square-wave current excitation is applied. The magnetic co-energy values in the motor's air gap are then calculated at equally spaced rotor shift angles, and the difference per unit angle determines the torque, as illustrated in Fig. 8. The motor speed variation curve is which shows in Fig. 9, showing the speed increasing from zero to the desired value of 300 RPM. Additionally, the phase currents of the motor over a limited time interval are presented in Fig. 10.

The comparison of copper and iron losses between the initially designed motor and the optimized motor with a 1:1:1:1 ratio, is shown in Fig. 11. The winding configuration, including conductor length and cross-sectional area, was precisely modeled in ANSYS/Maxwell according to standard BLDC motor design practices to ensure accurate calculation of copper losses [18].

The findings confirm that selecting motor efficiency and performance as the objective functions for dimension optimization significantly reduces losses in the optimized motor. In both the initial designed and the optimized motor, the electrical losses were calculated at the rated speed of 300 RPM and a rated torque of 25 N.m. These values were extracted using ANSYS software, providing a comprehensive analysis of the motor's performance.

Fig. 11 presents a comparison of these losses. Specifically, Fig. 11-(a) illustrates the variations in copper losses across different torque levels, while Fig. 11-(b) shows the core losses. Fig. 11-(c) highlights other losses, which include the combined frictional and windage losses, transistor losses, and diode losses. In addition, Fig. 11-(d) displays a bar chart of motor efficiency at various torque levels. According to this figure, the efficiency of the motor with the initial design at the rated torque is approximately 74%, whereas the optimized motor achieves an efficiency of around 86% at the same torque level.

5. CONCLUSION

This study presents an optimized design approach for concentrated winding Brushless DC (BLDC) motors tailored for aircraft actuator applications. Through detailed sensitivity analysis and finite element method (FEM) simulations, we have identified critical design parameters that significantly impact motor performance. The optimized BLDC motor prototype, with a 22-pole configuration and 24 stator slots, achieved a nominal torque of 22.5 Nm, which represents a 12.5% increase compared to the initial design specification of 20 Nm. Additionally, the motor's efficiency was enhanced to 86.4%, an improvement from the baseline efficiency of 74.2%. The torque ripple, a critical factor in actuator applications, was reduced to 1.8%, down from 4.6% in the non-optimized configuration. The motor's torque density was also increased by 10%, achieving 0.45 Nm/kg, compared to 0.41 Nm/kg in the preliminary design. These results demonstrate that the proposed optimization strategy effectively enhances the performance metrics of the BLDC motor, making it a more viable solution for high-precision applications in the aerospace industry. Future work will focus on further reducing manufacturing costs while maintaining the improved performance characteristics.

REFERENCES

- [1] G. Ellis, "Advances in brushless dc motor technology, control, and manufacture," in *Proc. Int. Intell. Motion Conf.*, pp. 267–267, INTERTEC INTERNATIONAL, INC, 1995.
- [2] H. M. Cheshmehbeigi and E. Karami, "Maximum output torque control in improved flux path homopolar brushless dc motor with axillary field by using optimal control of turn-on and turn-off angles in variable speed applications," *IEEE J. Emerging Sel. Top. Power Electron.*, vol. 6, no. 4, pp. 1722–1731, 2018.
- [3] S. Hajiaghasi, Z. Rafiee, A. Salemmia, and M. Aghamohammadi, "Optimal sensorless four switch direct power control of bldc motor," *J. Oper. Autom. Power Eng.*, vol. 7, no. 1, pp. 78–89, 2019.
- [4] M. Jafarboland and S. Mousavi, "Investigation of unbalanced magnetic force in permanent magnet brushless dc machines with diametrically asymmetric winding," *J. Oper. Autom. Power Eng.*, vol. 6, no. 2, pp. 255–267, 2018.
- [5] A. Infantraj, M. Augustine, E. F. I. Raj, and M. Appadurai, "Investigation of various laminating materials for interior permanent magnet brushless dc motor for cooling fan application," *CES Trans. Electr. Mach. Syst.*, vol. 7, no. 4, pp. 422–429, 2023.
- [6] L. Knypiński, A. Reddy, B. Venkateswararao, and R. Devarapalli, "Optimal design of brushless dc motor for electromobility propulsion applications using taguchi method," *J. Electr. Eng.*, vol. 74, no. 2, pp. 116–121, 2023.
- [7] F. Mahmouditabar, A. Vahedi, and N. Takorabet, "Robust design of bldc motor considering driving cycle," *IEEE Trans. Transp. Electr.*, vol. 10, no. 1, pp. 1414–1424, 2023.
- [8] J. Choi, J.-H. Lee, Y.-G. Jung, and H. Park, "Enhanced efficiency of the brushless direct current motor by introducing air flow for cooling," *Heat Mass Transfer*, vol. 56, pp. 1825–1831, 2020.
- [9] T. Anuja, M. A. N. Doss, R. Senthilkumar, K. Rajesh, and R. Brindha, "Modification of pole pitch and pole arc in rotor magnets for cogging torque reduction in bldc motor," *IEEE Access*, vol. 10, pp. 116709–116722, 2022.
- [10] S. B. Pandya, P. Jangir, M. Mahdal, K. Kalita, J. S. Chohan, and L. Abualigah, "Optimizing brushless direct current motor design: An application of the multi-objective generalized normal distribution optimization," *Heliyon*, vol. 10, no. 4, 2024.
- [11] D. Mohanraj, R. Arulavid, R. Verma, K. Sathiyasekar, A. B. Barnawi, B. Chokkalingam, and L. Mihet-Popa, "A review of bldc motor: state of art, advanced control techniques, and applications," *IEEE Access*, vol. 10, pp. 54833–54869, 2022.
- [12] V. Naeini and N. Sadeghi, "Optimum design of the outer rotor brushless dc permanent magnet motor with minimum torque ripples," *J. Oper. Autom. Power Eng.*, 2024.
- [13] N. Prabhu, R. Thirumalaivasan, and B. Ashok, "Critical review on torque ripple sources and mitigation control strategies of bldc motors in electric vehicle applications," *IEEE Access*, 2023.
- [14] G. H. Krishnan, C. M. Tejeswini, K. Gowtham, U. K. Chandra, P. Jyothsna, and U. R. Kanth, "Six-phase bldc motor design performance analysis for electric vehicle applications," in *2023 4th Int. Conf. Electron. Sustainable Commun. Syst.*, pp. 169–173, IEEE, 2023.
- [15] Y.-j. Park, J.-W. Kim, J.-H. Kang, J.-H. Ahn, S. Kim, and L. Ju, "Optimal design of bldc motor based on magnetic equivalent circuit considering the halbach magnet array," in *2022 IEEE 20th Biennial Conf. Electromagn. Field Comput.*, pp. 1–2, IEEE, 2022.
- [16] D. Hanselman, "Brushless permanent magnet motor design," 01 2003.

- [17] C. Tseng, W. Liao, and T. Tang, "Most user's manual, national chiao-tung university, taiwan, roc," tech. rep., Version 1.2, Tech. Rep. AODL-93-0, 1993.
- [18] N. Taran, D. M. Ionel, V. Rallabandi, G. Heins, and D. Patterson, "An overview of methods and a new three-dimensional fea and analytical hybrid technique for calculating ac winding losses in pm machines," *IEEE Trans. Ind. Appl.*, vol. 57, no. 1, pp. 352–362, 2020.